



Investigation of an Asymmetrical Rotor Hybrid Permanent Magnet Motor for Approaching Maximum Output Torque

Xianxian Zeng , Li Quan, Xiaoyong Zhu, *Member, IEEE*, Lei Xu, *Member, IEEE*, and Fangjie Liu 

Abstract—This paper presents a new asymmetrical rotor hybrid permanent-magnet (AR-HPM) motor with good torque performances. Different from the traditional symmetrical rotor structure, the asymmetrical rotor structure is employed to improve the torque production. This makes the reluctance torque and the magnetic torque reach the maximum at the same current phase angle. Based on the concepts, the motor is investigated by the finite-element method (FEM). The frozen permeability method (FPM) is applied to divide the torque into the reluctance torque and the magnetic torque. The electromagnetic characteristics and torque performances of the motor are compared with a conventional motor. The results show that the proposed design is efficacious in boosting output torque at the same operating conditions. Moreover, the results also demonstrate that the topology of the proposed AR-HPM motor features the advantage of avoiding the risk of demagnetization.

Index Terms—Asymmetrical rotor, ferrite-permanent magnet, hybrid permanent magnet brushless motor, rare-earth permanent magnet.

I. INTRODUCTION

RECENTLY, the electric vehicles (EVs) and hybrid electric vehicles (HEVs) have attracted much attention for being a promising solution to relieve the energy crisis. The rare-earth permanent magnet (RE-PM) motors with the advantages of high torque/power density and high efficiency play an important role in the EVs and HEVs applications [1]–[4]. However, the fluctuating price and unstable supply chain of RE-PM limits the further development of RE-PM motor. In order to cut down the volume of RE-PMs and obtain comparable torque performances, various approaches have been proposed [5], in which the hybrid PM motor (HPMM) is an effective solution. The HPMM adopts non-rare-earth PM material (e.g., ferrite PM) to replace RE-PM. The large amount of ferrite PMs are often arranged in spoke to make use of the limited rotor room [6]. Yet, in such kind of motors, the non-rare-earth PM often serves as main

magnetic sources, which maintains low BH product and limits the torque output capability to some extent. Consequently, the performances of HPMM are often inferior to the RE-PM motors. For improving output torque of the PM motor, rotor optimization are discussed in many literatures. A spoke hybrid PM motor in parallel is studied and compared with a conventional spoke ferrite motor in [7], the electromagnetic performances are improved, but the consumption of the NdFeB PM is higher. In [8], a spoke type ferrite PM motor with additional ferrite PM ring is proposed to improve the torque performance. In addition, the existing researches for HPMM are generally based on the premise that the rotor shape retains symmetrical topology. In general, by analyzing the torque components, the output torque is divided into PM torque (T_{PM}) and reluctance torque (T_{re}). It can be seen that the T_{PM} and T_{re} reach the peak value at different current angle. Yet, the torque components are not fully utilized, and various scholars and engineering pay a lot of attentions on the optimization of the motors for the torque component utilization [9], [10]. In [11], a V-type PM Motor with assisted barriers for improve the reluctance torque is investigated. In [12], an axial PM-assisted synchronous reluctance machine is presented, the rotor consist of reluctance motor and surface PM motor in axial direction, and it obtains a higher total torque and power factor. However, due to the complex magnetic circuit of the hybrid PM motor, the previous methods are not suitable for the hybrid PM motor.

In this paper, a new asymmetrical-rotor hybrid permanent magnet (AR-HPM) motor is proposed. In view of the concepts of the torque performances improvements, the magnetic torque and reluctance torque is adjusted to reach the peak value at nearly the same current phase angle based on the FEM analysis. In addition, a conventional hybrid PM motor with symmetrical rotor is introduced to verify the validity of the proposed topology under the same operating conditions.

II. MOTOR TOPOLOGY

A. Conventional Symmetrical Rotor Hybrid PM Motor

A conventional symmetrical rotor hybrid PM (SR-HPM) motor with spoke-type is applied as the referenced motor, as displayed in Fig. 1. The motor employs 12 stator slots with concentrated windings around the teeth, and the rare-earth PM (NdFeB) and non-rare-earth PM (Ferrite) are inserted alternately in circumferential symmetry as co-excitation sources.

Manuscript received July 28, 2018; accepted January 14, 2019. Date of publication January 17, 2019; date of current version February 11, 2019. This work was supported in part by the National Natural Science Foundation of China under Grant 51807081, Grant 51777089, Grant 51807080, and Grant 51877089 and in part by the Priority Academic Program Development of Jiangsu Higher Education Institutions. (Corresponding author: Xianxian Zeng.)

The authors are with the School of Electrical and Information Engineering, Jiangsu University, Zhenjiang 212013, China (e-mail: zxyff@ujs.edu.cn).

Color versions of one or more of the figures in this paper are available online at <http://ieeexplore.ieee.org>.

Digital Object Identifier 10.1109/TASC.2019.2893708

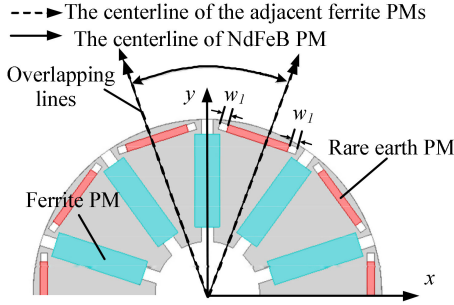


Fig. 1. SR-HPM motor.

TABLE I
SPECIFICATIONS OF THE REFERENCED MOTOR

Items	Unit	Value
Stator outer radius	mm	100
Air gap length	mm	0.5
Rotor outer radius	mm	60
Rotor inner radius	mm	36
Motor axial length	mm	68
Power	kW	5
Remanence of ferrite PM	T	0.41
Remanence of NdFeB	T	1.4

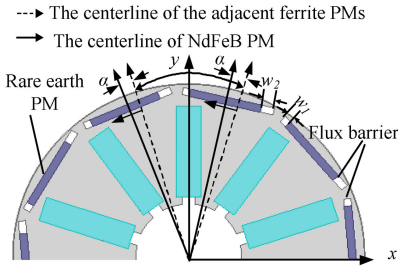
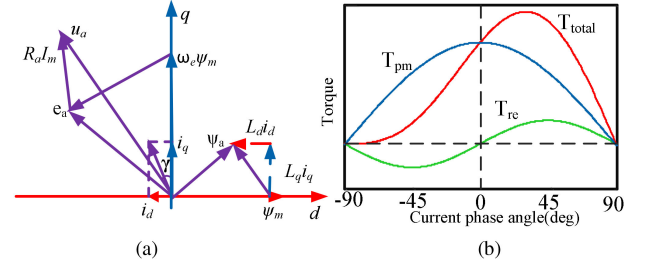


Fig. 2. Rotor topology of the AR-HPM motor.

Rare-earth permanent magnets are located in the middle of adjacent ferrites. The motor specifications are shown in Table I.

B. Proposed AR-HPM Motor

In conventional motor, the rotor is circumferential symmetry designed, thus the two axes, namely, the direct or d -axis and the quadrature or q -axis can be defined by Park transformation. The q -axis is 90° (electrical) from the d -axis. In the present motor, the principle is modified by asymmetry rotor, which is realized by associating the rare earth PM location and the flux barrier location design. Namely, the center line of the rare-earth PM is not coincides with that of the adjacent ferrite PMs. The stator of the proposed motor is identical to that of the referenced motor. Fig. 2 displays the asymmetry rotor design of the proposed motor, in which the spoke-type arrangement of the ferrite PM is unchanged, while the centerline of the rare-earth PM shift α angle to the q -axis and the flux barrier width are different for improving reluctance torque. That is, the d -axis location changes with respect to the q -axis. In addition, the proposed motor and the referenced motor make use of the identical volume of ferrite PMs and rare-earth PMs.

Fig. 3. Torque Characteristics of the basic model. (a) Vector diagram in the dq reference frame. (b) Torque characteristics.

C. Torque Characteristics

In the conventional permanent magnet synchronous motor, the electromagnetic torque can be obtained depending on the vector diagram derived from a dq rotor frame equivalent circuit using the Park transformation as shown in Fig. 3(a), the electromagnetic torque is expressed as:

$$T_{em} = T_{pm} + T_{re} = \frac{3p}{2} \left[\lambda_{pm} I_a \cos \theta + \frac{1}{2} (L_d - L_q) I_a^2 \sin 2\theta \right] \quad (1)$$

where T_{pm} is the magnetic torque, T_{re} is the reluctance torque, p is the number of pole pairs, I_a is the amplitude of the phase current, θ is the angle between the stator current vector and the q -axis designated as current phase angle, L_d and L_q are the inductances of the d -axis and q -axis, respectively, and λ_{pm} is the peak fundamental value of PM flux linking.

Based on (1), the typical torque characteristics are plotted, as shown in Fig. 3(b). To evaluate the contribution of the proposed design concept, a utilization factor (K) defined as the ratio between the utilized torque component and its corresponding peak torque component can be adopted as

$$UF_{PM} = \frac{T_{u,PM}}{T_{pk,PM}}; UF_{re} = \frac{T_{u,re}}{T_{pk,re}}; K = UF_{PM} \times UF_{re} \quad (2)$$

where $T_{u,PM}$ is the utilized torque produced PM, and $T_{u,re}$ is the utilized torque of reluctance torque. $T_{pk,PM}$ and $T_{pk,re}$ are the peak values of corresponding torque components.

Based on the FEM analysis, the motor design process is shown in Fig. 4. To enhance the torque component utilization ratio, the frozen permeability method (FPM) is applied. The initial and optimal parameters are listed in Table II.

III. RESULTS ANALYSIS

To fairly estimate the electromagnetic performances of the proposed motor, a motor is designed as a referenced motor which obtains overall the same dimensions with the AR-HPM motor. The specific design parameters of the two motors are listed in Table III.

A. Torque Characteristics

The torque characteristics of the referenced motor and the present motor versus the current phase angles are shown in Fig. 5, where the output torque is predicted by providing the

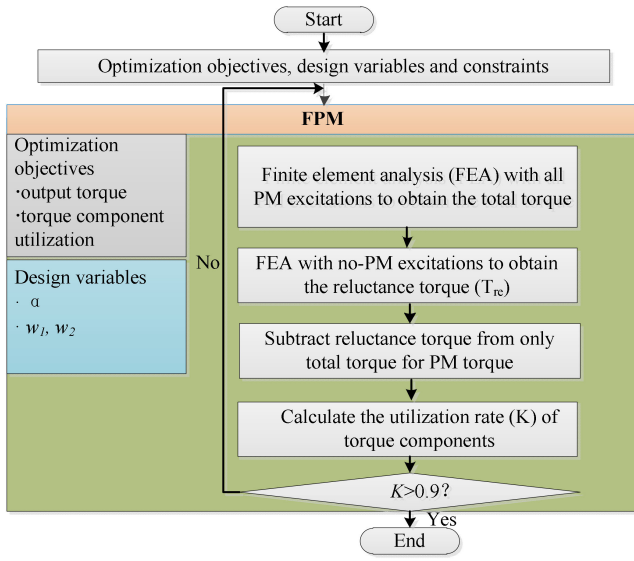


Fig. 4. Design and optimization flowchart of the AR-HPM motor.

TABLE II
OPTIMIZATION RESULTS OF THE MOTORS

Items	Unit	Optimal value	Constraint ranges
α	$^\circ$	3	$0^\circ \leq \alpha \leq 10^\circ$
w_1	mm	3	$1\text{mm} \leq w_1 \leq 5\text{mm}$
w_2	mm	4	$2\text{mm} \leq w_2 \leq 7\text{mm}$

TABLE III
COMPARISON RESULTS OF TWO MOTORS

Item	Unit	Referenced SR-HPM motor	Proposed AR-HPM motor
Outside stator diameter	mm	200	200
Inner stator diameter	mm	121	121
Axial length	mm	68	68
Stator yoke height	mm	8	8
Stator tooth height	mm	27	27
Stator tooth opening	mm	9	9
Outside rotor diameter	mm	120	120
Shifting angle	$^\circ$	0	3
Flux barrier width of two sides	mm	3/3	3/4
Ferrite PM volume	cm^3	176.8	176.8
NdFeB PM volume	cm^3	22.1	22.1
Rated phase current	A	40	40
Rated speed	rpm	1200	1200
Output torque	Nm	30.2	35.2
Ferrite type	-	Y30	Y30
Rare-earth type	-	NdFeB35	NdFeB35

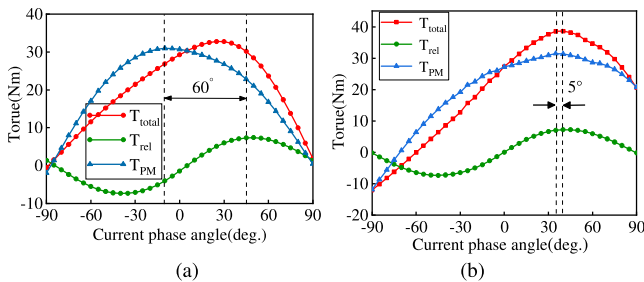


Fig. 5. (a) Torque characteristics of the SR-HPM motor. (b) Torque characteristics of the AR-HPM motor.

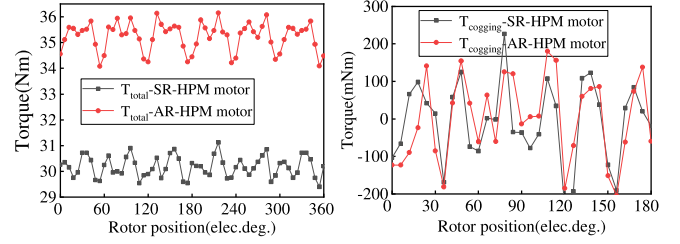


Fig. 6. Output torque and cogging torque of two motors.

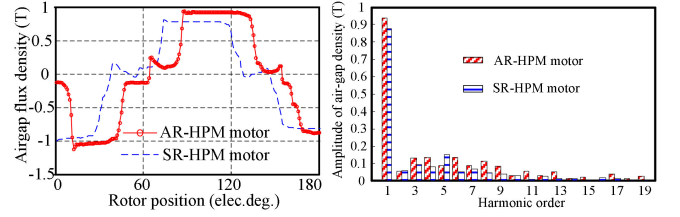


Fig. 7. Air gap density waveforms and FFT analysis of two motors. (a) Back-EMF. (b) FFT analysis.

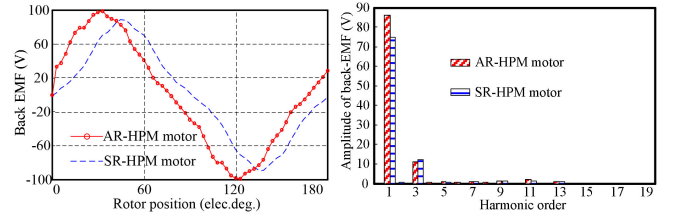


Fig. 8. Back-EMF waveforms and FFT analysis of AR-HPM motor and SR-HPM motor. (a) Back-EMF. (b) FFT analysis.

winding with sinusoidal current excitations density of 5 A/mm² at 1200 rpm. The results indicate that the magnetic torque and reluctance torque of the referenced model reach their maximum values at different current phase angles by 60° (elec.), whereas the two torque components of the proposed model reach the maximum values near the same current phase angle. From the Fig. 5(b) can be seen that the total torque versus the current phase angle of the proposed motor is higher than that of the referenced motor, which suggests the AR-HPM motor enjoys advantage of better torque output capability with the asymmetrical rotor topology.

The output torque and cogging torque comparison between the two motors are shown in Fig. 6. The average values of output torque of the AR-HPM motor increases by 16% compared with the SR-HPM motor. Besides, the cogging torque of the AR-HPM motor is approximately equal to that of SR-HPM motor.

B. Air-Gap Density and Back EMF

As primary electromagnetic performances, the air-gap flux density and no load back EMF comparison of the two motors are performed in Fig. 7 and Fig. 8. Fig. 7(a) shows the proposed motors obtains air gap density nearly 1.0 T, which higher than that of the referenced motor with 0.8 T. What that means, is the high PM utilization of the proposed motor. Because of the asymmetrical rotor, the air gap magnetic density waveform of the proposed motor is asymmetrical in one cycle, which is

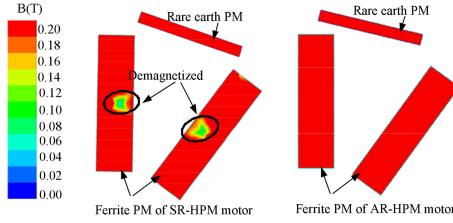


Fig. 9. Demagnetization irreversible demagnetization analysis.

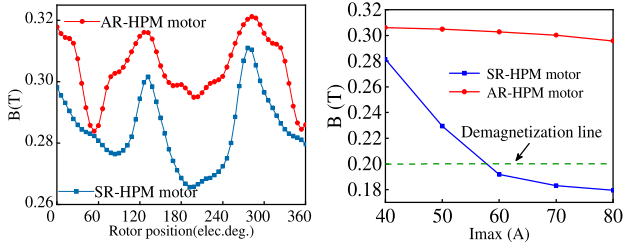


Fig. 10. (a) Operating points of ferrite PM under rated load. (b) Ferrite PM flux density versus different current.

different from the referenced motor. The corresponding fast Fourier transform (FFT) is displayed in Fig. 7(b).

It can be seen that the AR-HPM motor has higher fundamental components. Fig. 8(a) shows the proposed motor maintains higher back EMF amplitudes in phase than the referenced one, which suggests the proposed motor can provide higher output torque at the same phase current. It can be observed from Fig. 8(b) that the AR-HPM motor obtains higher air gap flux density fundamental magnitude.

C. Demagnetization Characteristics

Since ferrite-PM often suffers from irreversible demagnetization due to the inherent weakness of low coercivity, the demagnetization characteristics of the two motors are analyzed and compared in this section.

To qualitatively evaluate the partial irreversible demagnetization, Fig. 9 displays the partially demagnetized region of two motors reaches 1.5 times rated load. It can be observed that the ferrite PMs of the SR-HPM motor suffers demagnetization, while the counterparts of the AR-HPM motor avoid demagnetization. Thus it generally suggests that the proposed AR-HPM motor contains better anti-demagnetization capacity.

To further investigate the demagnetization characteristics, the flux densities of two motors are analyzed under rated load (40 A) and over load. Depending on the B-H curve of ferrite PM, it can be considered to be demagnetized when the flux density is lower than 0.2 T. It can be seen from Fig. 10(a) and Fig. 10(b) that the demagnetization line is drawn to estimate whether the PMs suffer from irreversible demagnetization. As presented in Fig. 10(a), both of the flux densities of the two motors under rated load are above the demagnetization limit and the operation points of the AR-HPM motor are higher than that of SR-HPM motor. However, when the load reaches 1.5 times the rated load, the ferrite PMs of the SR-HPM motor suffers from demagnetization, while the operation points of the AR-HPM motor is

still above the demagnetization line, which means the AR-HPM motor has better anti-demagnetization capability than AR-HPM motor under overload.

IV. CONCLUSION

A new design concept of asymmetric rotor is put forward for the spoke-type hybrid PM motor in this paper. Due to the asymmetric rotor, the magnetic torque and the reluctance torque reach the peak value near the same current phase angle and approach the maximum value of torque in theoretically. Hence, compared to the traditional symmetric rotor structure, the design of the asymmetric rotor structure can make full use of the torque components.

The electromagnetic characteristics and torque performances are investigated by the FEM. Compared with the referenced motor, the torque utilization rate of the proposed motor increases by 16%, and the cogging torque and torque ripple are nearly the same. The anti-demagnetization analysis result also shows that the proposed motor suffers low demagnetization risk. More detailed comparative results, optimization results, and experimental results will be given in the future presentation.

REFERENCES

- [1] X. Y. Zhu, J. Huang, L. Quan, Z. X. Xiang, and B. Shi, "Comprehensive sensitivity analysis and multi-objective optimization research of permanent magnet flux-intensifying motors," *IEEE Trans. Ind. Electron.*, vol. 66, no. 4, pp. 2613–2627, Apr. 2019.
- [2] X. Y. Zhu, Z. X. Xiang, L. Quan, W. Y. Wu, and Y. Du, "Multimode optimization design methodology for a flux-controllable stator permanent magnet memory motor considering driving cycles," *IEEE Trans. Ind. Electron.*, vol. 65, no. 7, pp. 5353–5366, Jul. 2018.
- [3] B. Ma, G. Lei, J. Zhu, Y. Guo, and C. Liu, "Application-oriented robust design optimization method for batch production of permanent-magnet motors," *IEEE Trans. Ind. Electron.*, vol. 65, no. 2, pp. 1728–1739, Feb. 2018.
- [4] B. Ma, G. Lei, J. Zhu, Y. Guo, and C. Liu, "Application-oriented robust design optimization method for batch production of permanent-magnet motors," *IEEE Trans. Ind. Electron.*, vol. 65, no. 2, pp. 1728–1739, Feb. 2018.
- [5] X. Y. Zhu, D. Y. Fan, L. H. Mo, Y. Y. Chen, and L. Quan, "Multiobjective optimization design of a double-rotor flux-switching permanent magnet machine considering multimode operation," *IEEE Trans. Ind. Electron.*, vol. 66, no. 1, pp. 641–653, Jan. 2019.
- [6] Q. C. G. H. Liu, and W. X. Zhao, "Design and analysis of the new high-reliability motors with hybrid permanent magnet material" *IEEE Trans. Magn.*, vol. 50, no. 12, Dec. 2014, Art. no. 8207010.
- [7] X. Wang, X. Y. Zhu, and C. Zhang, "Design and analysis of a spoke-type hybrid permanent magnet motor for electric vehicles," *IEEE Trans. Magn.*, vol. 53, no. 11, Nov. 2017, Art. no. 8208604.
- [8] M. Mohammad, K. Kim, and J. Hur, "Design and analysis of a spoke type motor with segmented pushing permanent magnet for concentrating air-gap flux density," *IEEE Trans. Magn.*, vol. 49, no. 5, pp. 2397–2400, May 2013.
- [9] X. Y. Zhu, W. Y. Wu, S. Yang, Z. X. Xiang, and L. Quan, "Comparative design and analysis of new type of flux-intensifying interior permanent magnet motors with different q-axis rotor flux barriers," *IEEE Trans. Energy Convers.*, vol. 33, no. 4, pp. 2260–2269, Dec. 2018.
- [10] G. H. Liu, G. H. Xu, W. X. Zhao, Z. Xiang, and X. X. Du, "Improvement of torque capability of permanent-magnet motor by using hybrid rotor configuration," *IEEE Trans. Ener. Conv.* vol. 52, no. 3, pp. 953–962, Sep. 2017.
- [11] W. L. Zhao, F. Zhao, T. A. Lipo, and B.-I. Kwon, "Optimal design of a novel V-type interior permanent magnet motor with assisted barriers for the improvement of torque characteristics," *IEEE Trans. Magn.*, vol. 50, no. 11, Nov. 2014, Art. no. 8104504.
- [12] W. L. Zhao, F. Xing, X. Wang, and T. A. Lipo, "Design and analysis of a novel PM-assisted synchronous reluctance machine with axially integrated magnets by the finite-element method," *IEEE Trans. Magn.*, vol. 53, no. 16, Jun. 2017, Art. no. 8104104.